Mon. Not. R. Astron. Soc. **000**, 1–11 (2007) Printed 14 April 2008 (MN LATEX style file v2.2)

Constraining the mass of the GRB 030329 progenitor⋆

Göran Östlin[1], Erik Zackrisson[2,1,3], Jesper Sollerman[1,4], Seppo Mattila[5,2], Matthew Hayes[1]
[1] *Stockholm Observatory, Department of Astronomy, Stockholm University, AlbaNova University Center, 106 91, Stockholm, Sweden*
[2] *Tuorla Observatory, University of Turku, Väisäläntie 20, FIN-21500 Piikkiö, Finland*
[3] *Department of Astronomy and Space Physics, Box 515, SE-75120 Uppsala, Sweden*
[4] *Dark Cosmology Centre, Niels Bohr Institute, University of Copenhagen, Juliane Maries Vej 30, 2100 Copenhagen, Denmark*
[5] *Astrophysics Research Centre, School of Mathematics and Physics, Queen's University Belfast, Belfast BT7 1NN, UK*
[6] *Geneva Observatory, University of Geneva, 51 chemin des Maillettes, 1290 Sauverny, Switzerland*

Accepted ... Received ...; in original form ...

ABSTRACT

The long-duration gamma-ray burst (GRB) 030329, associated with supernova (SN) 2003dh, occurred inside a star-forming dwarf galaxy at redshift $z = 0.1685$. The low redshift, and a rich set of archival Hubble Space Telescope (HST) images, makes this GRB well-suited for a detailed study of the stellar population in the immediate vicinity of the explosion. Since the lifetime of a star is directly tied to its mass, the age of the stellar population can be used to put constraints on the GRB and SN progenitor mass. From the HST images we extract the colours of the precise site from which the GRB originated, and find that the colours are significantly different from those of the overall host galaxy and the surrounding starburst environment.

We have used spectral evolutionary models, including nebular emission, to carefully constrain the age of the stellar population, and hence the progenitor, at the very explosion site. For instantaneous burst models we find that a population age of ∼5 Myr best matches the data, suggesting a very massive ($M_{\rm ZAMS} > 50\ M_{\odot}$) star as the progenitor, with an upper limit of 8 Myr ($M_{\rm ZAMS} > 25\ M_{\odot}$). For more extended star formation scenarios, the inferred progenitor age is in most cases still very young (< 7 Myr, implying $M_{\rm ZAMS} > 25\ M_{\odot}$), with an upper limit of 20 Myr ($M_{\rm ZAMS} > 12\ M_{\odot}$).

These age estimates are an order of magnitude lower than the ages inferred from the overall host galaxy colours, indicating that progenitor mass estimates based on data for spatially unresolved GRB host galaxies will in general be of limited use. Our results are consistent with the collapsar scenario.

Key words: Gamma rays: bursts – galaxies: starburst – galaxies: stellar content – stars: evolution GRB 030329, SN 2003dh

1 INTRODUCTION

It is now well established that long duration GRBs are connected to the deaths of massive stars. The standard picture is reviewed by Woosley and Bloom (2006), where the prevailing model is a collapsar (MacFadyden & Woosley 1999), i.e. a massive star collapsing to a black hole and producing an energetic supernova. The first piece of evidence for the supernova scenario came with the discovery of SN 1998bw in the error box of GRB 980425 (Galama et al. 1998; Patat et al. 2001), and was later confirmed by the association of GRB 030329 with SN 2003dh (Hjorth et al. 2003; Stanek et al. 2003; Matheson et al. 2003). It is generally assumed that the progenitors to these GRBs are very massive stars. Not all types of core-collapse SNe produce GRBs, and it is thought that only the upper mass range of the IMF is contributing to the GRBs. Moreover, the modeling of the properties of the supernovae accompanying the long GRBs points to very massive progenitors (e.g. Woosley and Bloom 2006). In the case of SN 2003dh, which was associated with GRB 030329, estimates in the range of 25 to 40 $M_{\odot}$ has been obtained from modelling the supernova observations (Mazzali et al. 2003; Deng et al. 2005).

Arguments for a massive stellar progenitor for long-duration GRBs also come from studies of the host galaxies. Fruchter et al. (2006) confirmed that the GRBs occur in blue star-forming galaxies, and are concentrated to the most active star forming regions. For some nearby supernovae not connected to GRBs, a study of the actual progen-

⋆ Based on observations with the NASA/ESA *Hubble Space Telescope*, obtained at the Space Telescope Science Institute, which is operated by the association of Universities for Research in Astronomy, Inc., under NASA contract NAS5-26555.

itor star has been possible. Recent programmes have taken a systematic approach to this question and have revealed several supernova progenitor stars in pre-explosion images (e.g. Smartt et al. 2004; Li et al. 2005; Gal-Yam et al. 2007). However, all the direct detections so far are for type II SNe with moderately massive progenitor stars. Furthermore, the progenitors of type Ib/c SNe still remain to be directly detected (e.g. Maund et al. 2005; Crockett et al. 2007) with the exception of SN 2006jc for which an outburst was observed coincident with the SN just two years before its explosion (Pastorello et al. 2007; Foley et al. 2007). For GRBs, which are typically more distant, we cannot detect single stars prior to explosion. An alternative way to probe the progenitor is to analyse the population of stars near the explosion site. Such modeling of the entire host galaxies has revealed that, overall, the stellar populations of GRB hosts are dominated by young stars. However, to put constraints on the actual GRB progenitor requires a close look at the very site where the GRB was born and exploded. A population study of the environment of GRB 980425 was carried out by Sollerman et al. (2005), who concluded that this GRB originated in a star more massive than 30 $M_{\odot}$. More recently, Thöne et al. (2007) found support for a massive star origin of the GRB 060505 which, however, did not have an associated luminous supernova. These results are consistent with the standard picture, although further and tighter constraints should be sought.

To probe the immediate environment of the explosions requires nearby bursts and/or high-resolution imaging. In this paper we investigate archival Hubble Space Telescope (HST) images obtained of the host of GRB 030329 at $z = 0.1685$ (Gorosabel et al. 2005). The host appears to be a subluminous ($L \sim 0.016L^{\star}$), metal-poor, galaxy with a star formation rate of $\sim 0.5\ M_{\odot}\ \mathrm{yr}^{-1}$ and a total stellar mass of $M \sim 10^8$–$10^9\ M_{\odot}$, dominated by a rather young stellar population (Gorosabel et al. 2005; Sollerman et al. 2005). The host galaxy will be further discussed in Sect. 4.2.

In this paper, we use the HST images to zoom in on the exact location of the GRB explosion. We show that useful constraints on the progenitor mass can be obtained by careful modeling of the colours as seen by HST. Such studies are complementary to e.g. modeling of the supernova component – and will help to constrain the properties of the exploding star.

In Sect. 2 we describe the observational material used. In Sect. 3 we describe how the optical data were analysed, i.e. how we subtracted the old population from the young star burst region. In Sect. 4 we describe the modeling of the stellar populations and discuss the constraints we derive on the progenitor. In Sect. 5 we discuss how age estimates can be improved and in Sect. 6 we summarise our conclusions.

Throughout the paper we are assuming the following cosmology: $\Omega_{\mathrm{M}} = 0.3$, $\Omega_{\Lambda} = 0.7$, $H_0 = 72\ \mathrm{km\ s^{-1}\ Mpc^{-1}}$.

2 OBSERVATIONS

All the data analysed in this paper have been retrieved from the Hubble Space Telescope (HST) data archive. Some of the images have previously been discussed by Sollerman et al. (2005) and Fruchter et al. (2006).

2.1 The ACS/WFC data

GRB 030329 was observed with the Wide Field Camera (WFC) of the Advanced Camera for Surveys (ACS) on several occasions between about two weeks after the explosion and more than two years subsequently. Since we are here interested in the properties of the host galaxy, early images are of little value except for pinpointing the exact GRB location. The images used in this paper are summarised in Table 1.

The drizzled F606W images were aligned to a common origin We co-added these images sorted in four temporal bins: 'early', 'mid', 'late' , and 'very late' (see Table 1). The 'early' images are useful for identifying the precise location of the GRB, but the afterglow contaminates the light from the host galaxy. In the 'mid' images, the afterglow has faded enough that these data can be used to study the host galaxy far from the explosion site. The 'very late' images contain no detectable afterglow or supernova light, and from comparing 'late' and 'very late' images, we conclude that 'late' images are safe to use also for the GRB environment. We made a total GRB-free image by masking out the GRB affected regions in the mid images and adding these to the late and very late images. In this way the final image has maximum depth in the outskirts of the host galaxy, but no afterglow or supernova contamination. The resulting image is shown in the upper left panel of Fig. 1. We used the same strategy to construct a GRB free image in F814W. For F435W we used the co-added images from a single 'late' dataset.

Photometric zero points were taken from the ACS www-pages[1] and are: 25.779, 26.398, 25.501 for the F435W, F606W and F814W filters, respectively, all in the VEGAMAG system, which will be adopted throughout this paper. In what follows we shall refer to magnitudes in this system as B_{435}, V_{606} and I_{814}. All data that is presented has been corrected for a foreground Galactic reddening of $E(B-V) = 0.025$ mag (Schlegel et al. 1998). Taking the different bandpass of the used filters with respect to the 'standard' system into account, the applied corrections are (in magnitudes): $A(B_{435}) = 0.109,\ A(V_{606}) = 0.075,\ A(I_{814}) = 0.049$.

2.2 The ACS/HRC/F250W data

The archive also contains several observations in the F250W filter with the UV-sensitive High Resolution Camera (HRC) of ACS, which were also retreived. However, we could not properly align the HRC/F250W observation with those obtained with the WFC. The different apertures of the two cameras results in slight inconsistencies in the astrometric keywords. As a result, we could not be sure that the MULTIDRIZZLE software had correctly registered the images at the requested pixel-level accuracy. Remaining misalignments could not be fixed by hand since no for- or background point-sources were available for the image registration. Hence, we did not use the F250W data in our final analysis.

[1] http://www.stsci.edu/hst/acs

Table 1. ACS/WFC images used (exposure time in seconds).

Filter	Date	Dataset name	Exp. time	Class
F606W	Apr. 15, 2003	J8IY2B021	400	early
F606W	Apr. 21, 2003	J8IY2J021	400	early
F606W	May 12, 2003	J8IY2M021	450	early
F606W	Nov. 12, 2003	J8IY2T010	1920	mid
F606W	Nov. 12, 2003	J8IY2T030	2088	mid
F606W	Feb. 4, 2004	J8IY2U010	1920	mid
F606W	May 25, 2004	J8IY9Z010	1920	late
F606W	May 25, 2004	J8IY9Z020	2080	late
F606W	May 9, 2005	J8IYF2010	1920	very late
F606W	May 9, 2005	J8IYF2030	2080	very late
F435W	May 24, 2004	J8IY9V010	1920	late
F814W	Nov. 12, 2003	J8IY2T050	2040	mid
F814W	May 24, 2004	J8IY9V020	2040	late

2.3 NICMOS data

GRB 030329 was also observed with the NIC2 camera of the NICMOS instrument onboard HST. These data suffered from well known artefacts in the form of non-linear temporal bias drifts during the exposures[2]. The data were re-reduced using the CALNICA pipeline and the artifacts removed using the BIASEQ and PEDSKY tasks of STSDAS. Unfortunately, the latest epochs which were the only ones free of GRB contamination suffered from cosmic ray persistence limiting the depth of these observations. Aligning the NIC2 images with ACS/WFC was complicated due to the very few reference sources visible within the NIC2 field of view. We therefore rotated the images to the orientation of the WFC data and used the GRB itself, present in the early NIC2 images, for centring. The images potentially relevant for our analysis are made up of two exposures in each of the F110W and F160W filters, taken on May 23, 2004. The total exposure time in each filter is 1216 s. However, only the F110W image turns out to be useful for our purposes, as further discussed in Sect. 3. The adopted NIC2+F110W zeropoint is 22.95 (VEGAMAG) and magnitudes will hereafter be denoted by J_{110}.

2.4 HST spectroscopic data

GRB 030329 was observed with both STIS and ACS in spectroscopic mode. It could potentially be very useful to constrain the internal extinction from the Hα/Hβ ratio at the actual location of the burst. However, these spectra[3] do not have enough signal, or are too heavily contaminated by the GRB afterglow at early epochs, to allow such an analysis.

3 PHOTOMETRIC ANALYSIS

We examined the shape of the host galaxy in the final very deep F606W image. We fitted ellipses to the outer isophotes and derived a luminosity profile by integrating in elliptic annuli. The structure of the outskirts of the host galaxy is well fitted by an exponential disk with scale length of $0\farcs3$ (0.9 kpc) and an inclination angle of $i = 55^\circ$ (assuming $\cos(i) = b/a$, i.e. an infinitely thin disk). We created a synthetic galaxy image with these properties, scaled to the surface brightness level of the outer parts of the host galaxy and subtracted it from the host galaxy image. In this way we obtained an image of the central starburst with no contamination from the underlying galaxy. The same method was used to obtain images of the central starburst in the F435W and F814W filters. Being cleaned from the underlying disk contribution, these images are suitable for a photometric modeling of the properties of the GRB explosion environment. In Fig. 1 we show the luminosity profile of the host and the resulting image after subtracting the underlying host galaxy.

We then proceeded to extract colours for the slightly off-centre GRB explosion site. In order to check how sensitive the results are to the host galaxy subtraction, we increased the luminosity of the disk model to the upper limit ('max disk') allowed by the uncertainties, and also derived the colours without subtracting an underlying disk ('no disk').

This photometric method is appropriate if the stellar population from which the GRB originated dominates the light within the aperture. An alternative method is to also subtract the median flux in a surrounding annulus, as is done in conventional aperture photometry, and this method was used as a consistency check.

The GRB environment photometry is presented in Table 2, and was extracted for an aperture radius of $r = 0\farcs1$. We also experimented with a smaller aperture which gave consistent results. For the $r = 0\farcs1$ photometry, aperture corrections of 0.510, 0.461 and 0.538 mag were subtracted from B_{435}, V_{606} and I_{814}, respectively (Sirianni et al. 2005).

The scaling of the underlying disk has a minor impact on the colours of the GRB explosion site. The statistical uncertainties are estimated to be $\sigma_B = 0.03, \sigma_V = 0.015, \sigma_I = 0.035$ magnitudes. The differences in Table 2 give a good idea about the systematic uncertainties, in which the subtraction (or not) of the local background has the largest impact. By modeling the stellar population (see Sect. 4.3) using the full range of values in Table 2, we also include the systematic uncertainties in our analysis.

In addition, we present in Table 3, the photometry for the whole galaxy.

3.1 NICMOS data

We were not able to clearly detect and fit the underlying host galaxy in the NICMOS images, but have extracted the flux in the GRB-region in apertures matching those of the WFC data. In the F160W image many pixels near the GRB explosion site are negative and we regard these data as unreliable and will not use them further. In the F110W image we could extract a magnitude for the same region as used for the WFC data but without subtraction of the underlying galaxy (corresponding to the 'no disk' option). In this way we obtained $J_{110} = 24.9 \pm 0.4$ mag., where we have adopted the definition of total NICMOS magnitudes and an aperture correction derived from the encircled energy distribution given in the HST/NICMOS Instrument Handbook (Barker et al. 2006).

[2] see http://www.stsci.edu/hst/nicmos
[3] http://www-int.stsci.edu/~fruchter/GRB/030329/index.html

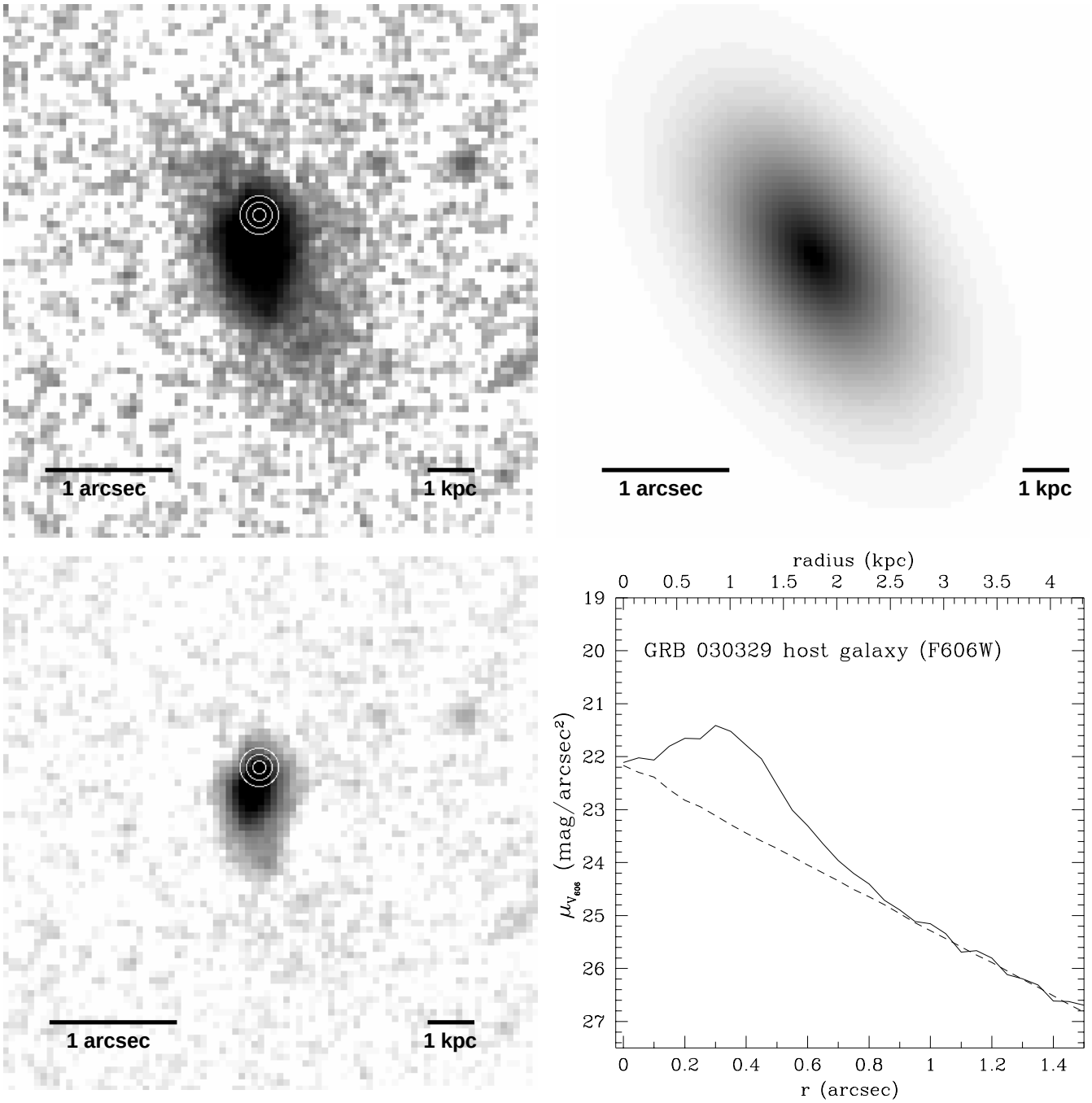

Figure 1. Upper left: The host galaxy of GRB 030329 in the F606W filter (HST/ACS). The field shown is $4\farcs2 \times 4\farcs2$ which corresponds to 12×12 kpc at the distance of GRB 030329. This image is made from data obtained at different epochs and is not contaminated by light from the GRB afterglow. The location of the GRB explosion is indicated by the concentric white circles (where the innermost circle corresponds to the used photometric aperture). **Upper right:** Synthetic exponential disk model fitted to the outer isophotes of the deep F606W image. The inclination is 55° and the scale length $0\farcs31$ (0.87 kpc). **Lower left:** Here we show the result of subtracting the disk model from the F606W image in the upper left panel. This has isolated a central starburst region, free of contamination from the underlying population described by the best fit disk model. The GRB occurred near the edge of the central starburst region, $\sim 0\farcs2$ from its centre. **Lower right:** The luminosity profile resulting from integrating the unsubtracted F606W image in the upper left panel in concentric ellipses (with centroid from the outer isophotes) is shown as a solid line while the fitted disk model is shown as a dashed line.

Table 2. GRB environment photometry. The upper entries are for photometry extracted in a 0.″1 radius aperture without subtracting the local background. For the lower entries, local background has been subtracted using the median value in one pixel wide annulus immediately outside the photometric aperture. All magnitudes are in the HST VEGAMAG system.

Disk model	Local backgr.	B_{435}	V_{606}	I_{814}	$B_{435}-V_{606}$	$V_{606}-I_{814}$
Max disk	no	24.843	24.778	24.237	0.066	0.540
Best disk	no	24.816	24.766	24.204	0.050	0.561
No disk	no	24.729	24.679	24.082	0.051	0.596
Max disk	yes	25.126	25.156	24.696	–0.044	0.480
Best disk	yes	25.114	25.159	24.678	–0.029	0.460
No disk	yes	25.117	25.116	24.610	0.002	0.506

Table 3. Integrated host galaxy photometry within the Holmberg radius (1.4″, equivalent to 3.9 kpc)

B_{435}	V_{606}	I_{814}	$B_{435}-V_{606}$	$V_{606}-I_{435}$
23.2	22.8	22.3	0.36	0.52

4 STELLAR POPULATION ANALYSIS

We will now describe how we use spectral evolutionary synthesis models together with the derived photometry to estimate the age of the stellar population. Once an age estimate has been found, this can be converted into a lower limit on the zero age main sequence progenitor mass ($M_{\rm ZAMS}$) using stellar evolutionary models from Meynet et al. (1994) and Fagotto et al. (1994). The lifetimes for these two independent models agree well, typically to within 5%. More recent calculations (Hirschi et al. 2004) that include stellar rotation indicate that, at least for solar metallicity, the effects on the life times are insignificant. For hypothetical, extremely rapidly rotating stars (e.g. Woosley and Heger 2006), the mass lifetime–relation could possibly be affected, but no quantitative estimates for such stars are yet available. In what follows we will adopt the Meynet et al. (1994) models. The models assume single star evolution, but even if the GRB progenitor were part of a binary system, this would have no major impact on the lifetime which is dominated by the main sequence phase.

4.1 Spectral synthesis

Integrated photometry is commonly analysed using spectral evolutionary synthesis models. In this procedure, it is important to adopt a model as closely adapted to the known physical properties of the target system as possible. As the GRB 030329 host galaxy is a blue object with strong emission-lines (Gorosabel et al. 2005), nebular emission is likely to give an important contribution to the optical spectrum. Many publicly available models do not include nebular emission and are therefore not suitable for analysing systems of this kind. The previous GRB 030329 host galaxy analysis by Gorosabel et al. (2005) is based on the Bruzual & Charlot (2003) model, which suffers from this shortcoming.

In the following, we adopt the Zackrisson et al. (2001) spectral evolutionary model, which uses the photoionisation code Cloudy version 90.05 (Ferland et al. 1998) to predict the nebular continuum and emission lines. For each time step, the spectral energy distribution of the stellar population is used as input to Cloudy, which makes the computation time-consuming, but provides a realistic evolution of the nebular component. The stellar component, which includes pre-main sequence evolution and a stochastic treatment of horizontal branch morphologies at low metallicities, is based on synthetic stellar atmospheres by Lejeune et al. (1998) and Clegg & Middlemass (1987), together with stellar evolutionary tracks mainly from the Geneva group. We have previously demonstrated (Östlin et al. 2003) that the Zackrisson et al. (2001) model performs much better than the publicly available version of the PÉGASE.2 code (Fioc & Rocca-Volmerange 1999) in reproducing the observed colours of young super star clusters. (Although PÉGASE.2 has previously been used in the analysis of long-duration GRB host, e.g. Sokolov et al. 2001; Sollerman et al. 2005.) This is thanks to its more sophisticated treatment of the nebular component which is known to contribute substantially. To allow an analysis of the broad-band magnitudes relevant for the current investigation, the spectra predicted by the models are redshifted to $z = 0.1685$ and convolved with the throughput curves of the filters used.

In the Zackrisson et al. (2001) model, the properties of the stellar component are regulated by the metallicity, initial mass function (IMF) and star formation history. We here assume the metallicity to be the same for the stars and the ionized gas, i.e. $Z = Z_{\rm stars} = Z_{\rm gas}$ and have explored $Z = 0.001, 0.004$ and 0.008. For IMF we have assumed a power-law ($\mathrm{d}N/\mathrm{d}M \propto M^{-\alpha}$) throughout the 0.08–120 $M_{\odot}$ stellar mass range, and we note that the actual slope at low masses ($M < 1\mathrm{M}_{\odot}$) will not affect the results for the young ages here considered. Our standard assumption is a Salpeter ($\alpha = 2.35$) IMF but we have also explored $\alpha = 1.85$ and 2.85. For simplicity, we assume the star formation rate (SFR) to be either instantaneous or exponentially decreasing over time ($\mathrm{SFR}(t) \propto \exp -t/\tau$), where the e-folding decay rate τ describes the duration of the star formation episode. An instantaneous burst corresponds to $\tau \approx 0$.

The properties of the nebular component are determined by the adopted hydrogen number density $n(\mathrm{H})$, which is assumed to be constant within the nebula, the gas filling factor f, and the gas mass $M_{\rm gas}$ available for star formation throughout the star formation episode. $M_{\rm gas}$ is used together with the adopted $\mathrm{SFR}(t)$ to determine the stellar Lyman continuum flux density for each time step. This be-

comes an important parameter, because the homology relation between plane-parallel nebulae with the same ionisation parameter (Davidson 1977) breaks down for the spherical nebulae assumed here.

The Zackrisson et al. (2005) model assumes that the nebula responds instantaneously to changes in the ionizing flux from the stellar population. This approximation holds as long as the many processes in the ionized cloud occur on timescales shorter than the age resolution that we are interested in. To ensure that this is not an issue, we used Cloudy to verify that the timescales of the longest radiative processes in the ionised gas are shorter than the time resolution of the stellar population model. For the range of gas parameters used in this paper, all processes occur on timescales much lower than 1 Myr, which is quite sufficient for our purposes.

4.2 The GRB 030329 host galaxy

The host galaxy of GRB 030329 has been investigated in several studies using ground based data. Gorosabel et al. (2005) used spectroscopy of the host to estimate a metallicity of $Z = 0.004$. However, (Sollerman et al. 2005) found that the available spectroscopy in the literature does not strongly constrain the metallicity of the host galaxy, and neither $Z = 0.001$ nor $Z = 0.008$ could be ruled out. Gorosabel et al. (2005) could not tightly constrain the extinction but found that the host galaxy spectral energy distribution and Balmer line ratios favoured $A_V \leqslant 0.6$. Matheson et al. (2003) used the colour of the GRB afterglow to infer $A_V = 0.12 \pm 0.22$. Extinction may vary spatially over a galaxy, and the GRB environment may well have a substantially lower extinction than that of the luminosity-weighted average of the host galaxy. This scenario also turns out to be consistent with our modelling results presented in Sect. 4.3.

In Fig. 2, we compare the colours of the overall host galaxy (filled triangle) to those of the GRB explosion site (filled square and circle, indicating colours with and without subtraction of the local background, respectively). While similar in $V_{606} - I_{814}$, the $B_{435} - V_{606}$ colour measured at the explosion site is bluer than for the host galaxy by ~ 0.3 magnitudes. The dereddening vectors relevant for the overall host galaxy (Gorosabel et al. 2005) and the GRB explosion sites (Matheson et al. 2003) are plotted as arrows. For the host galaxy, the two arrows included correspond to the extinction curves for the Milky Way and Small Magellanic Cloud (Pei 1992), respectively. For the GRB site, only one arrow has been plotted, because the two corrections overlap at this resolution. After correction, the GRB site is bluer than the host galaxy in $B_{435} - V_{606}$ but redder in $V_{606} - I_{814}$. As will be demonstrated, this is consistent with the notion that the stellar population hosting the GRB progenitor is substantially younger than that of the overall host galaxy.

The solid line in the left panel of Fig. 2 indicates the evolution predicted for a $Z = 0.004$, $\tau = 10^8$ yr, $M_{\rm gas} = 10^8\ M_\odot$ stellar population with gas parameters $f = 0.001$ and $n({\rm H}) = 10^2$ cm^{-3}. After reddening corrections, the host galaxy B_{435}, V_{606} and I_{814} data are consistent with a luminosity-weighted age of ≈ 50 Myr. This corresponds to the lifetime of a $\sim 8\ M_\odot$ star, which is close to the minimum progenitor mass for a core-collapse SN (Heger et al. 2003; Eldridge & Tout 2004). The collapsar scenario for long-duration GRBs requires a higher progenitor mass than this; a minimum mass of $\sim$25–30 $M_\odot$ is required in order for stars to have cores that collapse to black holes and to have sufficient angular momentum to form a disk (Heger et al. 2003).

Age estimates for composite stellar populations based on optical broadband photometry alone are typically not very precise. This is due to the degeneracy between star formation history and age (e.g. Gil de Paz & Madore 2002; Zackrisson et al. 2005), and, for systems with ongoing star formation, because of uncertainties in the physical conditions of the ionised interstellar medium (e.g. Zackrisson et al. 2001). These effects are demonstrated in the right-hand panel of Fig. 2, where the B_{435}, V_{606} and I_{814} data are compared to the predicted evolution for a model identical to the one in the left panel, except for a slightly shorter star formation episode ($\tau = 5 \times 10^7$ yr) and a lower hydrogen density ($n({\rm H}) = 10$ cm^{-3}). In this case, the best-fitting age becomes as small as 1–2 Myr. The large difference between the evolution in the two panels of Fig. 2 at low ages is entirely due to changes in the nebular spectrum. Since we have little information on the exact star formation history of the host galaxy and its detailed gas properties, the optical broadband data simply do not contain sufficient information to constrain the age with very high precision.

An age higher than 50 Myr is nonetheless favoured by the ground based near-IR data of Gorosabel et al. (2005). This is illustrated in Fig. 3, where the temporal evolution of various model sequences are compared to their $V - H$ measurement for the GRB 030329 host galaxy. In all cases, the best-fitting ages lie around ≈ 100 Myr, which is broadly consistent with Gorosabel et al. (2005). The ages inferred from $V - H$ are relatively robust to changes in the assumed nebular gas parameters.

While a best-fitting age of ~ 100 Myr would correspond to a GRB progenitor mass much lower than that favoured by the collapsar scenario, stars with much younger ages – and hence higher masses – would still be present in a population with on going star formation (i.e. $\tau > 0$). Hence, while the integrated host galaxy properties are broadly consistent with a collapsar, they do not provide useful constraints on the mass of the actual GRB progenitor.

4.3 The GRB explosion site and the age of the GRB progenitor

Starburst regions often contain young star clusters, sometimes referred to as 'super star clusters' (SSCs) with absolute magnitudes $M_V < -10$ (Arp & Sandage 1985; Meurer et al. 1995). At closer look, luminous starburst regions are often composed of numerous SSCs of varying age (Östlin et al. 2003). Each such SSC must have formed on a short timescale (McKee & Tan 2002) and they are commonly assumed to be truly single stellar populations, even if the star formation history of a whole starburst region may be more complex. A nearby example is R136, the central cluster of the 30 Doradus complex which Massey & Hunter (1998) found to be well explained by a star formation episode of duration up to 4 Myrs and a standard Salpeter IMF.

The restframe absolute magnitude of the GRB explosion site is $M_{V_{606}} \approx -14.8$ which indicates a stellar popu-

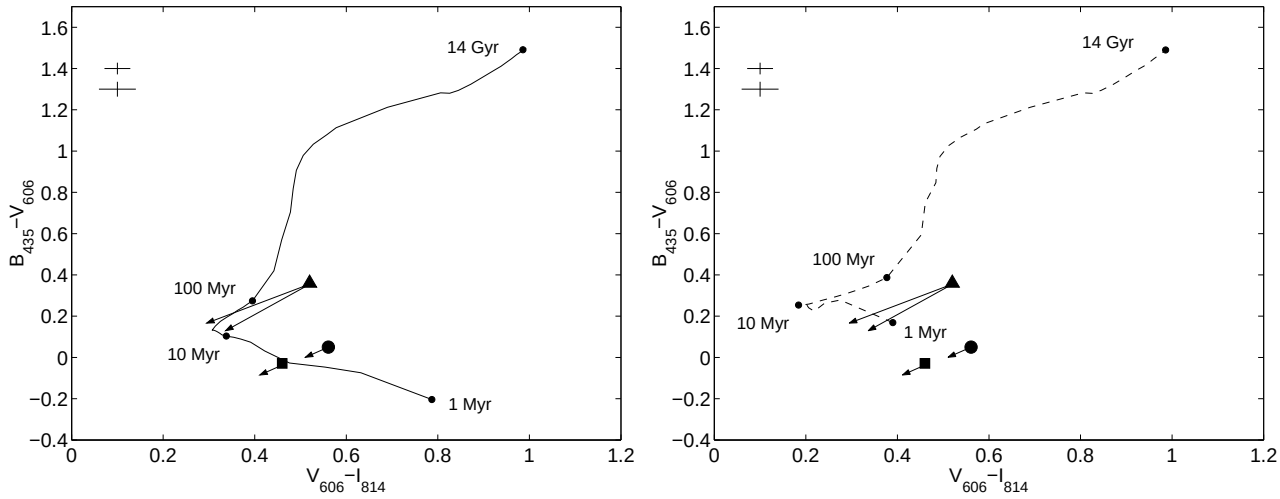

Figure 2. The $V_{606} - I_{814}$ vs. $B_{435} - V_{606}$ colours of the integrated GRB 030329 host galaxy (filled triangle) and the GRB explosion site (filled square and circle, indicating the colours with and without subtraction of the local background). The arrows indicate the dereddening vectors for Milky Way and Small Magellanic Cloud extinction curves (Pei 1992), given the extinction estimates of Gorosabel et al. (2005) for the overall galaxy and Matheson et al. (2003) for the explosion site. At this resolution, the two arrows overlap in the latter case. The smaller cross in the upper left corner indicates the $1\,\sigma$ statistical uncertainties of the host galaxy colours, whereas the larger cross indicates the uncertainties for the GRB explosion site. **Left:** The solid line represents the spectral evolution predicted for a burst-like stellar population at $z = 0.1685$ with $Z = 0.004$, $\tau = 10^8$ yr, $M_{\rm gas} = 10^8\ M_\odot$, $f = 0.001$ and $n({\rm H}) = 10^2$ cm^{-3}. The dots along this line indicate ages of 1 Myr, 10 Myr, 100 Myr and 14 Gyr. After reddening correction, the host galaxy is consistent with an age of ~ 50 Myr. **Right:** The dashed line represents the predicted evolution for a population with $\tau = 5 \times 10^7$ yr and $n({\rm H}) = 10$ cm^{-3}, but parameter values otherwise identical to those in the left hand panel. In this case, the best-fitting age becomes only 1–2 Myr, demonstrating the degeneracies involved in determining accurate ages for young stellar populations from optical broadband photometry only.

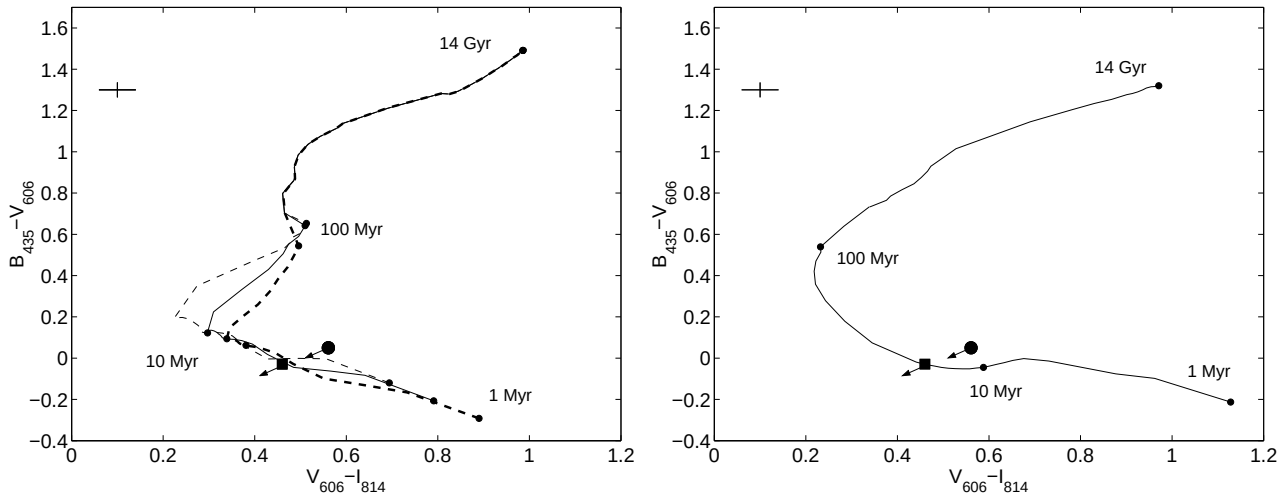

Figure 4. The $V_{606} - I_{814}$ vs. $B_{435} - V_{606}$ colours of the GRB 030329 explosion environment (as in Fig. 2, filled square and circle represent colours derived with and without subtraction of the local background) compared to various model populations (lines). The extinction corrections are the same as in Fig. 2. **Left:** Stellar populations with exponentially decreasing star formation rates of $\tau = 5 \times 10^6$ (thin dashed), 10^7 (thin solid) and 2×10^7 yr (thick dashed). All scenarios assume $Z = 0.004$, $M_{\rm gas} = 10^7\ M_\odot$, $f = 0.001$ and $n({\rm H}) = 10^2$ cm^{-3}, leading to a best-fitting age of less than 10 Myr. **Right:** A stellar population with $Z = 0.001$, but with parameters otherwise identical to the $\tau = 10^7$ yr scenario from the left hand panel. In this case, the best-fitting age becomes ≈ 15 Myr.

lation mass of $\sim 10^6\ M_\odot$ (the exact value depends on the actual age and reddening). Our extraction radius ($0.1''$) corresponds to 0.28 kpc and the GRB exploded at the eastern edge of the highest surface brightness region in the starburst (see Fig. 1 and also **?**). Hence it may have occurred in a single very luminous SSC, or in a complex of several SSCs of more 'normal' luminosity.

If the GRB occurred in a single SSC, then the star formation time scale (τ) should be close to instantaneous (or have a maximum τ of a few Myr), after which negative feedback associated with photo-ionisation and stellar winds would have quenched further star formation. However, our aperture may include more than one SSC in projection, and their different ages could then mimic a temporally extended star formation event. In the nearby blue compact galaxy ESO 338–04, the central 2 kpc starburst is composed of more

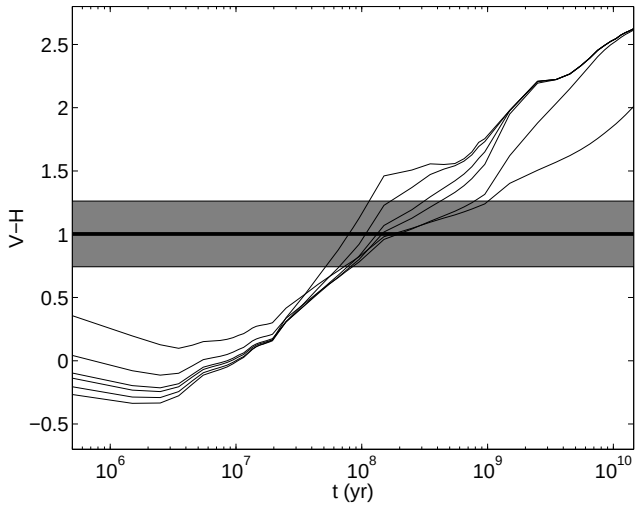

Figure 3. The temporal evolution in $V-H$ predicted by various models compared to the ground-based data by Gorosabel et al. (2005) for the host galaxy (thick solid line, with grey region indicating $1\,\sigma$ error bars). The observed colour has been corrected for Galactic and intrinsic extinction – the latter assuming the Gorosabel et al. (2005) extinction estimates and a Small Magellanic Cloud extinction curve. The different model predictions correspond to star formation histories $\tau = 5\times10^7$, 10^8, 2×10^8, 3×10^8, 10^9, 10^{10} yr (from top to bottom at an age of $\sim 5\times10^8$ yr). A population with $Z = 0.004$, $M_{\rm gas} = 10^8\ M_\odot$, $f = 0.01$ and $n({\rm H}) = 10^2$, cm^{-3} has been assumed throughout. Regardless of model scenario, the best-fitting age lies around ~ 100 Myr.

than 50 young SSCs with ages ranging from new-born to about 40 Myr (Östlin et al. 2003). If the situation is similar in the host galaxy of GRB 030329, then the effective star-formation time-scale (τ) in our aperture could be extended up to 10–20 Myr. This uncertainty on τ is the most serious limitation for our method and is directly tied to the spatial resolution and distance of the target. Below we shall discuss the constraints on the age of the GRB progenitor for various values of τ and other parameters.

The left panel of Fig. 4 shows that the GRB explosion site can be well-fitted by a $Z = 0.004$, $M_{\rm gas} = 10^7\ M_\odot$ population with a star formation time scale around $\tau = 10^7$ yr. Contrary to the case for the overall host galaxy, the age of the GRB environment appears to be very young – well below 10 Myr (corresponding to $M_{\rm ZAMS} > 21\ M_\odot$). Just as in the case of the host galaxy, the exact age is uncertain because of the aforementioned effects related to star formation history and properties of the ionized interstellar medium. In Fig. 4, three different star formation histories are plotted ($\tau = 5\times10^6$, 10^7 and 2×10^7 yr). All of these scenarios provide reasonable fits to the observed colours of the GRB site, but at slightly different ages (2–5 Myr).

The variations in the colours predicted by these scenarios at such early stages of evolution come from the different Lyman continuum flux densities that these stellar populations produce. While the best-fitting ages for the GRB environment are systematically lower than those for the overall host galaxy, it is still possible to find a small number of model parameter combinations that would allow higher than 10 Myr. This is demonstrated in the right panel of Fig. 4, where the metallicity of the $\tau = 10^7$ yr scenario from the left panel has been changed to $Z = 0.001$, giving an age of 14 Myr. This is actually the highest best-fitting age found when fitting the B_{435}, V_{606}, I_{814} and J_{110} magnitudes of the GRB environment to the 100 sets of model parameter values explored. It corresponds to a GRB progenitor mass of $M_{\rm ZAMS} \geqslant 15\ M_\odot$. We once again stress, that because of the adopted $\tau > 0$ star formation history, the GRB progenitor may in this case have a lifetime anywhere in the range from 3 to 14 Myr, i.e. fully consistent with the collapsar scenario of Heger et al. (2003).

As shown in Sect. 4.2, near-IR data can be very useful for improving age estimates based solely on optical photometry. In Fig. 5 we compare the $V_{606} - J_{110}$ colours of the GRB environment with the evolution predicted for different values of τ. Colours with (thick solid line) and without (thick dashed line) subtraction of the local background are shown. Due to the large photometric uncertainties, a best-fitting age of anywhere from 0 to 20 Myr can be derived from this colour. The quality of the J_{110} data is obviously too poor to substantially improve the age estimates.

In all, 100 models were fitted to the data in Table 2. The variations in colours between the different photometry methods give a good representation of the systematic uncertainties, whereas the statistical uncertainties are always small, with the exception of the J_{110}-band. We compare the various photometries (thus spanning the range of systematic uncertainties) to the models and select those solutions that match the data to within $3\,\sigma$ of the statistical uncertainties. The extinction has been a free parameter in the fit, but all fits within $3\,\sigma$ of the photometric uncertainties consistently produced small values: $E(B_{435} - V_{606}) < 0.1$ mag. This is consistent with the value derived from the optical afterglow (Matheson et al. 2003), which is reassuring.

For the 40 instantaneous burst models explored, we find that all models that provide good fits (within $3\,\sigma$ of the photometric uncertainties) indicate a very young progenitor: the best fit is always less than 5 Myr (implying $M_{\rm ZAMS} \geqslant 47$ M$_\odot$) and the $3\,\sigma$ upper limit is 8 Myr ($M_{\rm ZAMS} \geqslant 26$ M$_\odot$).

Following the discussion above, we now also consider 60 additional models with more extended star formation episodes, $\tau \leqslant 50$ Myr. The best fitting ages are in general still very young with the vast majority at $\leqslant 5$ Myr. However a small number (1 to 3, depending on which photometry is used) of models give decent fits for ages 7–14 Myr ($M_{\rm ZAMS} > 30$ to 15 M$_\odot$), with $3\,\sigma$ upper limits of 20 Myr ($M_{\rm ZAMS} > 12$ M$_\odot$). One of these models has already been presented in Fig. 4 (right panel).

Of all the 100 models with $\tau \leqslant 50$ Myr, 30–50% (depending on which photometry is used) provide best fit solutions that are within the $3\,\sigma$ statistical limits. On average the photometry that provides the best fit to the models is the 'Best disk' without subtraction of the local background. The vast majority of models that produce good fits give very young ages ($\leqslant 5$ Myr). However, since we cannot rule out the physical parameters for those few that give higher ages, we are left with a rather loose mass constraint for the progenitor.

We note that if we would have adopted the rather common approach of simply assuming an instantaneous burst with fixed metallicity and standard IMF and gas parameters, our constraints would have appeared as very tight.

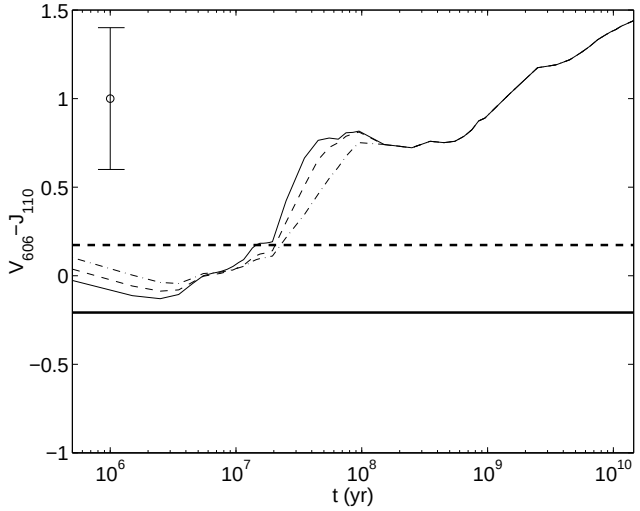

Figure 5. The temporal evolution in $V_{606} - J_{110}$ predicted by various model scenarios compared to the colour of the GRB explosion site with (thick solid line) and without (thin dashed line) subtraction of the local background. The open symbol in the upper left indicates the statistical $1\,\sigma$ uncertainty. The observed colours have been corrected for Galactic and intrinsic extinction – the latter assuming the Matheson et al. (2003) estimate and a Small Magellanic Cloud extinction curve. The difference between Milky Way, Small and Large Magellanic Cloud extinction curves (Pei 1992) only amount to an uncertainty of 0.02 magnitudes in this colour. The different model predictions correspond to star formation histories $\tau = 5 \times 10^6$ (solid line), 10^7 (dashed) and 2×10^7yr (dash-dotted). A population with $Z = 0.004$, $M_{\rm gas} = 10^7\ M_\odot$, $f = 0.001$ and $n({\rm H}) = 10^2$, cm^{-3} has been assumed throughout. Due to the uncertainty in the subtraction of the local background, a best-fitting age of anywhere from 0 to 20 Myr can be derived, and within the error bars, ages of up to 100 Myr are in fact allowed. Such high ages are however inconsistent with the $B_{435} - V_{606}$ and $V_{606} - I_{814}$ colours.

Instead, we have conservatively explored a large parameter space in order to really test the power of this method.

5 OUTLOOK

As we have shown, the GRB 030329 environment is best fitted by an age $\leqslant 5$ Myr, which is an order of magnitude lower than the age inferred for the overall host galaxy. This implies that progenitor mass estimates based on spectral or photometric data for poorly resolved host galaxies may be of limited value. Even with the high-resolution data analysed here, the uncertainties in the exact star formation history and gas properties of the GRB environment impose severe limits on the precision with which the mass of the GRB progenitor can be derived from broadband photometry.

An additional source of uncertainty stems from the intrinsic accuracy of the spectral evolutionary model used. Currently, the only way to assess such uncertainties would be to analyze the data using several different models in parallel. As we have shown that the treatment of nebular emission is very important for the age derived for the GRB 030329 environment, only models including a nebular component (e.g. Moy et al. 2001; Anders & Fritze-v. Alvensleben 2003; Magris et al. 2003; Dopita et al. 2005) should be used in such a comparison.

To better constrain the GRB progenitor masses more diagnostics are required. As already shown in Fig. 5, better quality near-IR data would be quite useful. This could be obtained with NICMOS, the next generation HST optical/IR imager WFC3, or with ground based adaptive optics systems. It would also be very useful to complement the optical HST data with a V-like filter that does not transmit the [OIII]$_{\lambda\lambda 4959,5007}$ emission line, since this would make the analysis less sensitive to assumed nebular gas parameters.

The equivalent width of the Hα emission line, EW(Hα), measured through spectroscopy or narrow-band photometry, may also provide useful constraints. In Fig. 6, we present the EW(Hα) evolution predicted by the Zackrisson et al. (2001) model during the first 50 Myr of a burst-like stellar population for three different star formation histories. For a given EW(Hα) measurement, the youngest age is inferred by the shortest star formation episode (here represented by an instantaneous burst), whereas the oldest age is inferred from the longest period of star formation considered ($\tau = 2 \times 10^7$ yr). Even without detailed knowledge of the star formation history, interesting age constraints can be derived from EW(Hα). If, for instance, EW(Hα)$\approx$ 1000 Å, the allowed age range would be 3–8 Myr, corresponding to a progenitor star in mass the range 25–120 $M_\odot$. For EW(Hα)$\approx$ 100 Å, a lower limit of 8 Myr could be imposed, indicating a progenitor mass below 25 $M_\odot$. Moreover, the EW(Hα) of a young stellar population is almost completely insensitive to many of the parameters used in the Zackrisson et al. (2001) model to regulate the properties of the ionized gas.

While being a powerful age indicator, the Hα equivalent width comes with a number of potential caveats that require consideration: While insensitive to the *gaseous* metallicity, there is a certain dependence on the *stellar* metallicity. This is demonstrated in Fig. 6, where we contrast the EW(Hα) evolution at $Z_{\rm stars} = Z_{\rm gas} = 0.001$, 0.004 and 0.008. Without more detailed metallicity information than this, the age constraints derived from the EW(Hα)$\approx$ 1000 Å and 100 Å measurements would be weakened to 3–20 Myr and $\geqslant 7$ Myr, respectively. Emission-line diagnostics formally probe the gaseous metallicity, which may differ somewhat from the stellar counterpart, and this will be a lingering source of error in the conversion from EW(Hα) to population age.

Selective extinction, i.e. the possibility that the emission line and the continuum originate from different spatial regions with different dust content (e.g. Calzetti et al. 1994), represents another potential complication.

This investigation provides support for the origin of long duration GRBs in very massive stars. In Sollerman et al. (2005) we found a similar conclusion for SN 1998bw (GRB 980425). The parent population of core collapse supernovae is expected to be biased towards ages corresponding to the lifetime of stars with mass close to the lower limit for SNe ($\sim 8 M_\odot$), since for a normal IMF these are more common than very massive stars. Already the finding that two of the still few known SNe coincident with long duration GRBs seem to have higher masses suggests that the parent populations may be different. This is consistent with studies of the spatial distribution of GRBs and SNe within galaxies (Fruchter et al. 2006). It also agrees with the modeling of the SNe associated with GRBs, which typically indicate

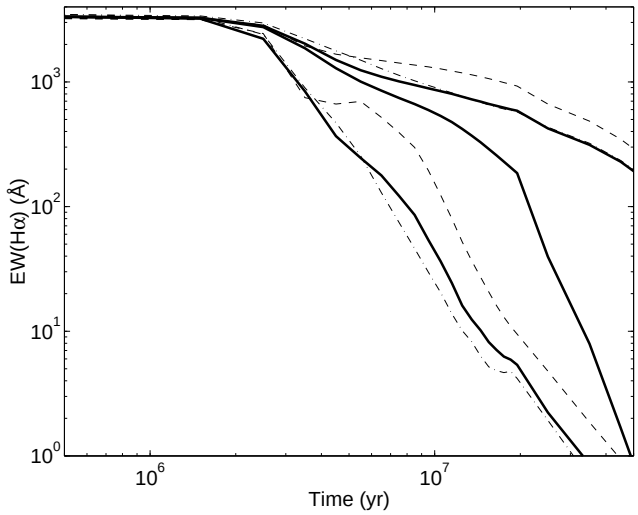

Figure 6. The temporal evolution of the Hα emission-line equivalent width predicted for stellar populations with burst-like star formation histories. The thick solid lines correspond to $Z = 0.004$ populations with exponentially decaying star formation rates of $\tau \approx 0$ (i.e. instantaneous burst), 5×10^6 and 2×10^7 yr (from bottom to top at an age of 10^7 yr). The two thin dashed (dash-dotted) lines represent the corresponding equivalent width predictions for $\tau \approx 0$ and $\tau = 2 \times 10^7$ yr when instead $Z = 0.001$ ($Z = 0.008$).

very massive progenitors (e.g. Mazzali et al. 2007, Table 1). Admittedly more examples would be needed since for individual cases there is always a risk that photometry is affected by limited spatial resolution and chance projections such that the progenitor had a different age than its surroundings. By imaging the most nearby GRB host galaxies with HST-like resolution, population studies of the explosion environment can provide statistical constraints on GRB progenitor masses. The method could also be used for supernovae that are too distant for single stars in their host galaxies to be resolved ($D > 20$ Mpc) and has been used for constraining the progenitors of the type IIP SN 2004dj (Maíz-Apellániz et al. 2004; Wang et al. 2005) and the type Ic SN 2007gr (Crockett et al. 2008)

6 SUMMARY

We have used archival HST images to derive photometry for the explosion site of GRB 030329. This has been used together with spectral evolutionary synthesis models, including nebular emission and a wide variety of parameter settings, to constrain the age of the stellar population. Taking this age to equal the lifetime of the GRB progenitor star, we can use the tight relationship between initial mass and lifetime to weigh the progenitor.

Studying the photometry at the resolution allowed by HST, the explosion site has an inferred age of $\leqslant 5$ Myr for an instantaneous burst assumption. The $3\,\sigma$ upper limit of 8 Myr corresponds to a minimum progenitor mass of 25 $M_\odot$, in line with the predictions of the collapsar model for the origin of long duration GRBs (Heger et al. 2003).

The main limitation is related to spatial resolution (for $z = 0.1685$ one HST/ACS/WFC pixel corresponds to 140 pc) and arises because we cannot be sure that the GRB parent population can be described by a single stellar population. Thus, nearby clusters of different age may contaminate the photometry, thereby mimicking an extended star formation history. Allowing for a more extended star formation history, most models still predict a minimum progenitor mass of around 25 $M_\odot$, but for a small number of models the minimum allowed (within $3\,\sigma$) progenitor mass is $\leqslant 12 M_\odot$.

We discuss ways to obtain tighter age constraints and identify the equivalenth width of Hα and near-IR photometry as useful additional diagnostics.

If exercised on a sufficient number of long duration GRBs, the method in this paper could provide information on the progenitor mass and metallicity distributions. This would provide an independent comparison to estimates obtained through modeling of the associated supernova.

ACKNOWLEDGEMENTS

G.Ö. acknowledges support from the Swedish Research Council (VR) and the Swedish National Space Board. E.Z. acknowledges support from VR, the Royal Swedish Academy of Sciences (KVA) and the visitor programme at the Dark Cosmology Centre, where a large part of this work was carried out. The Dark Cosmology Centre is funded by the Danish National Reserach Foundation. G.Ö. and J.S. acknowledges a grant from the Crafoord foundation, administrated through KVA. The work of S.M., conducted as part of the award "Understanding the lives of massive stars from birth to supernovae" made under the European Heads of Research Councils and European Science Foundation EURYI (European Young Investigator) Awards scheme, was supported by funds from the Participating Organisations of EURYI and the EC Sixth Framework Programme, and also the Academy of Finland (project: 8120503).

REFERENCES

Anders, P., Fritze-v. Alvensleben, U. 2003, A&A 401, 1063
Arp H., Sandage A., 1985, AJ, 90, 1163
Barker E., Pirzkal N., et al. 2006, "NICMOS Instrument Handbook", Version 9.0, (Baltimore, STScI)
Bruzual, G., & Charlot, S. 2003, MNRAS, 344, 1000
Calzetti, D., Kinney, A. L., & Storchi-Bergmann, T., 1994, ApJ 429, 582
Clegg, R. E. S, & Middlemass D., 1987, MNRAS 228, 759
Crockett, R. M., Smartt, S.J., Eldridge, J.J., et al. 2007, MNRAS, 381, 835
Crockett, R. M., Maund, J.R., Smartt, S.J., et al. 2008, ApJ 672, L99
Davidson, K. 1977, ApJ, 218, 20
Deng J., Tominaga N., Mazzali P.A., Maeda K., Nomoto K., 2005, ApJ 624, 898
Dopita, M. A., Groves, B. A., Fischera, J., et al. 2005, ApJ, 619, 755
Fagotto F., Bressan A., Bertelli G., Chiosi C., 1994, A&AS 105, 29
Eldridge, J. J., & Tout, C. A. 2004, MNRAS 353, 87
Ferland, G. J., Korista, K. T., Verner, D. A., Ferguson, J. W., Kingdon, J. B., & Verner, E. M. 1998, PASP, 110, 761

Fioc M., & Rocca-Volmerange B., 1999, astro-ph/9912179
Fruchter A.S., Levan A.J., Strolger L., et al., 2006, Natur 441, 463
Foley, R. J., Smith, N., Ganeshalingam, M., Li, W., Chornock, R., & Filippenko, A. V. 2007, ApJ 657, L105
Galama T.J., Vresswijk P.M., van Paradijs J., et al. 1998, Natur 395, 670
Gal-Yam, A., Leonard, D.C., Fox, D.B., et al. 2007, ApJ, 656, 372
Gil de Paz, A. & Madore, B. F. 2002, AJ 123, 1864
Gorosabel, J., Perez-Ramirez D., Sollerman J., et al. 2005, A&A, 444, 711
Heger, A., Fryer, C. L., Woosley, S. E., Langer, N., & Hartmann, D. H. 2003, ApJ 591, 288
Hirschi R., Meynet G., Maeder A., 2004, A&A 425, 649
Hjorth J., Sollerman J., Møller P., et al., 2003, Natur 423, 847
Li, W., Van Dyk, S. D., Filippenko, A. V., & Cuillandre, J.-C. 2005, PASP 117, 121
Lejeune, T., Cuisinier, F., & Buser, R., 1998, A&AS 130, 65L
MacFadyen A.I., & Woosley S. E 1999, ApJ, 524, 262
Maíz-Apellániz, J., Bond, H. E., Siegel, et al., 2004, ApJ 615, L113
Magris C. G., Binette, L., & Bruzual A. G. 2003, ApJS, 149, 313
Massey P., Hunter D.A., 1998, ApJ 493, 180
Matheson, T., Garnavich P.M., Stanek K.Z., et al. 2003, ApJ, 599, 394
Maund J. R., Smartt S.J., 2005, MNRAS 360, 288
Maund, J. R., Smartt, S. J., & Schweizer, F. 2005, ApJ 630, L33
McKee C.F., Tan J.C., 2002, Natur 416, 59
Meurer G.R., Heckman T.M., Leitherer C., Kinney A., Robert C., Garnett D.R., 1995, AJ 110, 2665
Meynet, Maeder A., Schaller G., Scaerer D., Charbonnel C., 1994, A&AS 103, 97
Moy, E., Rocca-Volmerange, B., & Fioc, M. 2001, A&A, 365, 347
Mazzali, P., Deng, J., Tominaga, N., et al. 2003, ApJ, 599, L95
Mazzali, P., Nomoto, K., Maeda, K., Deng, J., 2007, RevMexAA, 30, 23
Östlin, G., Zackrisson, E., Bergvall, N., Rönnback, J. 2003, A&A, 408, 887
Östlin, G., Cumming, R.J., Bergvall, N., 2007, A&A, 461, 471
Pastorello, A., Smartt, S.J., Mattila, S., et al. 2007, Nature 447, 829
Patat F., Cappellaro E., Danziger J., et al., 2001, ApJ 555, 900
Pei, Y. C. 1992, ApJ, 395, 130
Schlegel D.J., Finkbeiner D.P., Davis M., 1998, ApJ 500, 525
Sirianni M., Jee M.J., Benitez N., et al., 2005, PASP 117, 1049
Smartt S.J., Gilmore G.F., Trentham N., Tout C., Frayn C.M., 2001, ApJ 556, L29
Smartt, S. J., Maund, J. R., Hendry, M. A., et al., 2004, Science, 303, 499
Sokolov, V.V., Fatkhullin, T.A., Castro-Tirado, A.J., et al., 2001, A&A, 372, 438
Sollerman, J., Östlin, G., Fynbo, J. P. U., Hjorth, J., Fruchter, A., & Pedersen, K. 2005, New. Astron. 11, 103
Stanek K.Z., Matheson T., Garnavich P.M., et al. 2003, ApJ 591, L17
Thöne, C.C., Fynbo, J.P.U., Östlin G., et al., 2007, accepted to ApJ (astro-ph/0703407)
Wang, X., Yang, Y., Zhang, T., Ma, J., Zhou, X., Li, W., Lou, Y.-Q., & Li, Z. 2005, ApJ, 626, L89
Woosley S.E., Bloom J.S., 2006, ARA&A 44, 507
Woosley S.E., Heger A., 2006, ApJ 637, 914
Zackrisson, E., Bergvall, N., Olofsson, K., Siebert, A. 2001, A&A, 375, 814
Zackrisson, E., Bergvall, N., Östlin, G. 2005, A&A, 435, 29